FLUID-SOLID MUTIPHASE NUMERICAL SIMULATION ON LOCAL SCOUR BELOW A WEIR USING COUPLING METHOD OF E-MPS AND DEM

TAKAYOSHI HIGUCHI
Department of Civil and Environmental Engineering, Gunma University, Japan
Pacific Consultants Co., Ltd., Chiyoda-ku, Tokyo, Japan, takayoshi.higuchi@tk.pacific.co.jp

TAKAHIRO SAITOH
Department of Civil and Environmental Engineering, Gunma University, Japan, t-saitoh@gunma-u.ac.jp

YOSHIHIKO SHIMIZU
Department of Civil and Environmental Engineering, Gunma University, Japan, shimz@ce.gunma-u.ac.jp

ABSTRACT

Riverbed degradation occurs in many rivers of Japan. It damages river crossing structures, such as weirs and groundsills, with backward facing steps. If a large flood occurs in such a situation, it is feared that the blocks protecting the riverbed will be washed away due to local scour downstream from the structures. We conducted a vertical two-dimensional numerical simulation of local scour occurring downstream from river crossing structures. Local scour is a complex phenomenon due to the interaction between flow and sediment; therefore, advanced numerical simulations are necessary for expressing such dynamic behavior. A coupling method of the Explicit Moving Particle Simulation (E-MPS) method and the Discrete Element Method (DEM) has been developed to overcome the difficulty. The E-MPS method is a particle method that the implicit computational scheme of the conventional MPS method for the pressure Poisson equation is solved by explicitly. To investigate the applicability of the present coupling method to local scour occurring downstream from river crossing structures, we compared the numerical results from the present method simulation with those from the movable-bed hydraulic model experiment we conducted.

Keywords: local scour, weir, groundsill, E-MPS, DEM

1. INTRODUCTION

Riverbed degradation is occurring in many rivers of Japan due to the decrease in sediment supply from upstream. When riverbed degradation occurs downstream from river crossing structures, such as weirs and groundsills with backward facing steps, the decrease in flow momentum that was assumed at the time of their construction no longer occurs, resulting in damage to the protection blocks downstream when there is a flood. Also, embankments may collapse due to the destruction of river crossing structures. Therefore, evaluation of the destruction limit of river-crossing structures is an important issue for disaster prevention.

Yamamoto et al. (2018) carried out a movable-bed hydraulic model experiment to understand the destruction phenomena caused by riverbed degradation downstream of a groundsill protected with blocks. In that study, the relationship between the occurrence of groundsill breakage and hydraulic conditions was organized as a matrix of unit-width flow rate and downstream water level, and the following two points were reported. The first is that the local scour downstream of the groundsill expanded and the riverbed lowered with the increase in the unit-width flow rate and lowering of the downstream water level. The second is that the outflow of the upstream blocks spreads following the outflow of the downstream-end blocks, and destruction progressed quickly. Nakagawa et al, (1987) described other destruction phenomena of a bed protection such as "sucking sand out of gaps in blocks of bed protection", "piping", and "direct impact of falling water and boulders". However, as Yamamoto et al. (2018) reported, the most catastrophic destruction phenomenon of weirs and groundsills is the sudden destruction from the downstream-end protection blocks. It is due to what increases the difference between the upstream and downstream water levels when it occurs the riverbed degradation downstream from the weirs and the groundsills. Therefore, studying the destruction limit is an important issue. Conducting an experiment every time to evaluate the destruction limit takes time and effort. Therefore, it is preferable to construct a numerical analysis technique that can predict and evaluate such the destruction phenomenon.

The destruction phenomenon of weirs and groundsills is a phenomenon in which flow conditions, riverbed,

and bed-protection blocks interact dynamically. Therefore, it is difficult to apply Computational Fluid Dynamics (CFD) using the Eulerian approach, which has been used in the past. In this study, we focused on the particle method using a Lagrangian method for the fluid phase. A typical particle method is the Moving Particle Simulation (MPS) method (Koshizuka and Oka (1996)), and we used the Explicit MPS (E-MPS) method (Oochi et al. (2010)). The E-MPS method is one of the MPS method and the implicit computational scheme of the conventional MPS method for the pressure Poisson equation is solved by explicitly. With MPS method, it is possible to calculate the local scour phenomenon downstream from river crossing structures and the flow that follows the outflow of bed-protection blocks, as targeted in this study, because it does not require using an Eulerian mesh. However, it is difficult to evaluate pressure with such methods (Oochi et al. (2011)). For the solid phase, we used the Discrete Element Method (DEM) (Cundall and Strack (1979)), which is a Lagrangian method. The Lagrange-Lagrange method by coupling the MPS method with the DEM was developed and applied to practical engineering problems (Yamada and Sakai (2013)) and (Harada et al. (2019)).

We first conducted a movable-bed hydraulic model experiment to explain local scour. Next, as a first step in the development of a numerical technique to evaluate the destruction limit of bed protection, we combined the E-MPS method with the DEM (E-MPS/DEM) for solving the fluid-solid multiphase flow problem, which takes into account the interaction between flow and riverbed. To investigate the applicability of E-MPS/DEM to local scour phenomenon downstream of weirs, we compared the numerical results of the simulation with those from the movable-bed hydraulic model experiment.

2. MOVABLE-BED HYDRAULIC MODEL EXPERIMENT

2.1 Experimental method

We conducted the movable-bed hydraulic model experiment on a weir with an integrated concrete structure. Figure 1 shows the model diagram. The channel where the weir was constructed was 700 cm long, 50 cm high, and 40 cm wide. The length of the main weir was 3.0 cm, the length of the apron 10.0 cm, and the height of weir was 2.0 cm. Riverbed sections were installed downstream of the weir; the length of the flat section was 29.0 cm, that of the 1/12.5 slope section was 50.0 cm, and that of the 1/350 slope section was about 400.0 cm. The unit-width flow rate q from upstream was 0.012 m^2/s. The outflow from the downstream end of the channel was free outflow. The water-flow time was 10 minutes. The grain size of the sand was 0.76 mm. The sand was not supplied from upstream.

2.2 Experimental results and discussion

Figure 2 (a) shows the conditions of the riverbed before water flow, and Figures 2 (b), (c), (d), (e) and (f) show the flow conditions during water flow and the occurrence of local scour 24 sec, 25 sec, 26 sec, 3 min, and 10 min after water flow, respectively. At each time step, a water level difference occurred between the weir and riverbed due to the occurrence of scour, resulting in a jet flow. Huffmans (1998) mentioned that many different forms of jet flow can occur, e.g., attached jet, wave jump, and surface jet. In this experiment, we confirmed that scour occurs while the jet flow changes between attached jet and wave jump. At 24 sec (Figure 2 (b)), the jet flow was close to attached jet, and the maximum scour depth z_d was 2.8 cm and scour length L was 16.0 cm. At 25 sec (Figure 2 (c)), the jet flow was close to wave jump, and z_d was 2.3 cm and L was 17.5 cm. At 26 sec (Figure 2 (d)), the jet flow was again close to attached jet, and z_d was 2.3 cm and L was 18.5 cm. While changing the jet flow, scour expanded not only at the flat section but also due to riverbed variation on the 1/12.5-slope section, as shown in Figures 2 (e)–(f). At 3 min (Figure 2 (e)), z_d was 8.5 cm and L was 33.0 cm. At 10 min (Figure 2 (f)), the scour reached the bottom of the channel, and z_d was 10.0 cm and L was 54.0 cm. We confirmed that the scour length greatly expanded when the jet flow became attached jet.

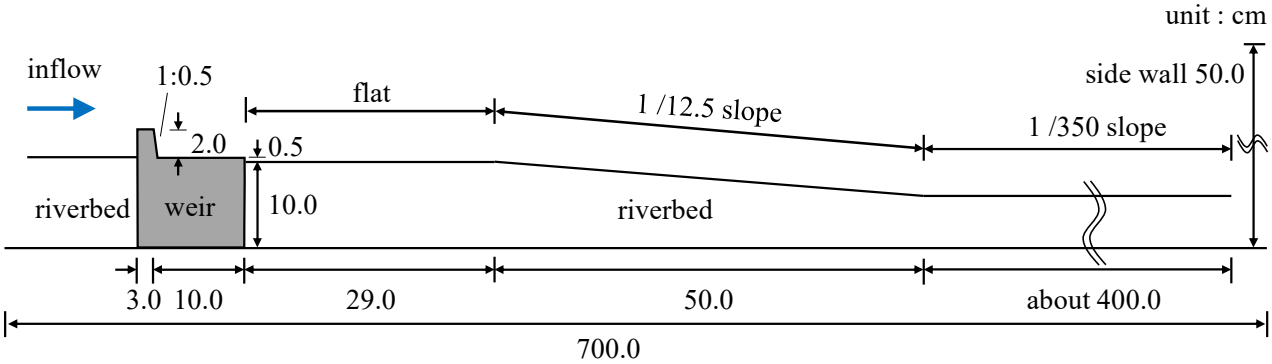

Figure 1. Sectional view of the movable-bed channel

When the jet flow was close to wave jump, the expansion of the scour tended to stagnate, as shown in Figure 2 (c). We also confirmed that the erosion of the upstream face of the scour significantly progressed because the jet flow was directed vertically downward, depending on the situation.

As described above, the scour phenomenon is a phenomenon in which the scour shape changes and the jet flow changes accordingly within a short time. The scour shape changes due to the change in the jet flow. In other words, the scour phenomenon is a phenomenon that expands when the flow interacts with the riverbed. We investigated the applicability of E-MPS/DEM to the scour phenomenon by conducting vertical two-dimensional numerical simulation.

3. NUMERICAL MODELING

3.1 Overview

The target phenomenon in this study is not a phenomenon in which the solid phase of the riverbed mixes with the fluid phase and the fluid can move violently in the riverbed. Therefore, in the calculation of the fluid phase with E-MPS/DEM, the solid phase is treated as a wall surface until it separates from the riverbed. The solid phase separated from the riverbed was relatively small compared to the volume of the fluid phase in the above experiment. In such a case, the supply of momentum from the solid phase to the fluid phase is small, and the momentum loss of the fluid phase is small. Hence, the flow velocity of the fluid phase is not much different from the case of a single phase containing no solid phase. Only the momentum supply from the fluid phase to the solid phase is modeled with E-MPS/DEM to drive and track the solid-phase particles. However, since the solid phase, which changes over time, is taken treated as a wall, the effect on the fluid phase due to changes in the riverbed composed of the solid phase is also taken into account. E-MPS/DEM adopts a simple method in which solid particles that have once separated from the riverbed are not treated as a wall surface.

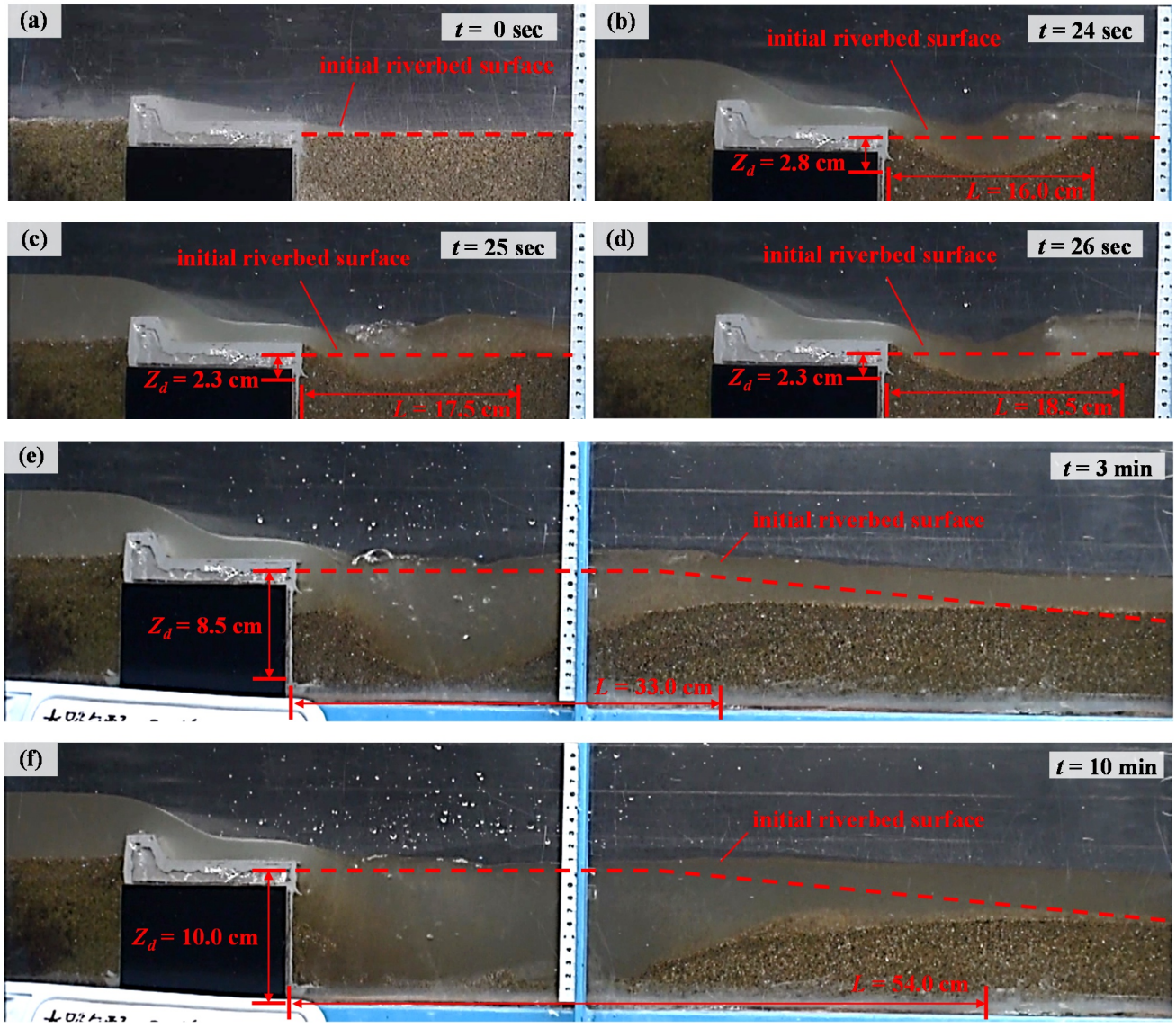

Figure 2. Experimental results

3.2 Governing equations

3.2.1 Fluid phase

The particle method is a calculation method that approximates the motion of a continuum by the motion of discrete particles and does not require an Eulerian mesh, as does the Finite Difference Method (FDM) and Finite Element Method (FEM). Since it is also a Lagrangian method for calculating moving particles, there is no need to calculate the advection term, which is particularly effective for analysis involving large deformation of interfaces such as water and riverbed surfaces. Since the volume of the solid phase in the fluid phase is relatively small compared to the volume of the fluid phase, the same formula is used for the fluid phase as in the case of the single phase. For the fluid phase, the governing equations are continuity and Navier-Stokes equations, which are written as follows:

$$\frac{D\rho}{Dt} + \rho\nabla \cdot \boldsymbol{u} = 0 \tag{1}$$

$$\frac{D\boldsymbol{u}}{Dt} = -\frac{1}{\rho}\nabla P + \nu\nabla^2\boldsymbol{u} + \boldsymbol{g} \tag{2}$$

where ρ, t, $\boldsymbol{u}$, P, ν, and $\boldsymbol{g}$ are the density, time, fluid velocity vector, fluid pressure, kinematic viscosity, and gravity acceleration, respectively.

3.2.2 Solid phase

For the solid phase, the governing equation for the solid particles is written using Newton's second law of translational and rotation motion as follows:

$$m_s\frac{d\boldsymbol{v}_s}{dt} = \boldsymbol{F}_c + \boldsymbol{F}_f + \boldsymbol{F}_P + \boldsymbol{F}_g \tag{3}$$

$$\boldsymbol{I}\frac{d\omega}{dt} = \boldsymbol{T} \tag{4}$$

where m_s, $\boldsymbol{v}_s$, $\boldsymbol{F}_c$, $\boldsymbol{F}_f$, $\boldsymbol{F}_P$, $\boldsymbol{F}_g$, $\boldsymbol{I}$, ω, and $\boldsymbol{T}$ are the mass of the solid particle, solid particle velocity vector, contact force, fluid force, fluid pressure, gravity force, momentum of inertia, angular velocity, and torque, respectively. With E-MPS/DEM, $\boldsymbol{F}_P$ in Eq. (3) is calculated by a simple method considering only buoyancy by using the specific gravity in water as the density of solid particles.

3.3 Modeling of fluid phase

3.3.1 Particle number density

The MPS method calculates the interaction between fluid particles by introducing a weight function $w(r)$. $w(r)$ defined by Yamada et al. (2013) can be written as follows:

$$w(r) = \begin{cases} \dfrac{r_e}{r} + \dfrac{r}{r_e} - 2 & (r < r_e) \\ 0 & (r \geq r_e) \end{cases} \tag{5}$$

where r is the distance between two particles. Interactions are restricted to an effective radius r_e. The particle number density n_i is written using the positions $\boldsymbol{r}_i$ and $\boldsymbol{r}_j$ of a particle i and its neighboring particle j as follows:

$$n_i = \sum_{j\neq i} w\left(|\boldsymbol{r}_j - \boldsymbol{r}_i|\right) \tag{6}$$

The density ρ_i is written assuming that it is proportional to the sum of the weight function as follows:

$$\rho_i = \frac{n_i}{n_0} \tag{7}$$

where n_0 is the particle number density under the incompressible condition, which is calculated in advance. With E-MPS/DEM, a wall boundary of the non-slip condition is simulated in the same manner as with the existing MPS method by arranging fixed wall particles. As described above, E-MSP/DEM treats solid particles as wall particles until they separate from the riverbed. The arrangement of wall particles with the MPS method is a lattice arrangement, as shown in Figure 3 (a), but in the case of solid particles, the arrangement is often a packed arrangement, as shown in Figure 3 (b). Therefore, there arises a problem in that the density of the wall boundary becomes discontinuous. With E-MPS/DEM, the particle number density when handling solid phase particles is modified from Eq. (6) as follows:

$$n_i = \sum_{j\neq 1}^{fluid} w\left(|\boldsymbol{r}_j - \boldsymbol{r}_i|\right) + \sum_{j\neq 1}^{wall} w\left(|\boldsymbol{r}_j - \boldsymbol{r}_i|\right) + \sum_{j\neq 1}^{solid} w\left(|\boldsymbol{r}_j - \boldsymbol{r}_i|\right)\frac{n_0}{n_{s0}} \tag{8}$$

(a) lattice arrangement (b) packed arrangement

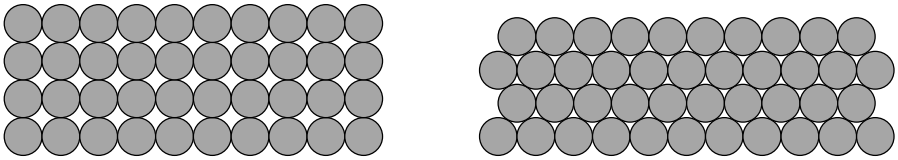

Figure 3. Particle arrangement

where n_{s0} is the particle number density under the incompressible condition of solid particles, which is calculated in advance.

3.3.2 Pressure calculation

With the E-MPS method, the fluid is allowed to be slightly compressed, and the pressure is calculated as a function of density as follows:

$$P_i = \begin{cases} c^2 \dfrac{\rho_0}{n_0}(n_i - n_0) & (n_i > n_0) \\ 0 & (n_i \le n_0) \end{cases} \tag{9}$$

where c is the speed of sound. The weight function $w_g(r)$ used in the pressure gradient term defined by Yamada et al. (2013) as follows:

$$w_g(r) = \begin{cases} \dfrac{r_e}{r} - \dfrac{r}{r_e} & (r < r_e) \\ 0 & (r \ge r_e) \end{cases} \tag{10}$$

The gradient ∇ included in the first term on the right in Eq. (2) is discretized using the particle interaction model between particles i and j as follows:

$$\langle \nabla P \rangle_i = \frac{d}{n_{g0}} \sum_{j \ne i} \left[\frac{(P_j + P_i)(\boldsymbol{r}_j - \boldsymbol{r}_i)}{|\boldsymbol{r}_j - \boldsymbol{r}_i|^2} \right] w_g(|\boldsymbol{r}_j - \boldsymbol{r}_i|) \tag{11}$$

where d is the number of dimensions and n_{g0} is a particle number density under the incompressible condition, calculated using a different weight function for the pressure gradient $w_g(r)$.

3.3.3 Viscosity term

The Laplacian ∇^2 included in the second term on the right in Eq. (2) is discretized using a particle interaction model between particles i and j as follows:

$$\langle \nabla^2 \boldsymbol{u} \rangle_i = \frac{2d}{\lambda_0 n_0} \sum_{j \ne i} [(\boldsymbol{u}_j - \boldsymbol{u}_i) w(|\boldsymbol{r}_j - \boldsymbol{r}_i|)] \tag{12}$$

where λ_0 is the weighted average of square distance.

3.4 Modeling of solid phase

3.4.1 Contact model

The $\boldsymbol{F}_c$ in Eq. (3) is modeled by the interaction between particles with a linear spring, friction slider, and dashpot. The $\boldsymbol{F}_c$ between solid particles i and j is decomposed into normal and tangential acting forces $\boldsymbol{F}_{cn}$ and $\boldsymbol{F}_{cs}$, respectively. In the tangential direction, the condition to slide when the force is more than the limit is given. The $\boldsymbol{F}_{cn}$ and $\boldsymbol{F}_{cs}$ are given as follows:

$$\boldsymbol{F}_{cn} = k_n \boldsymbol{\delta}_n + \eta_n \dot{\boldsymbol{\delta}}_n \tag{13}$$

$$\boldsymbol{F}_{cs} = \begin{cases} k_s \boldsymbol{\delta}_s + \eta_s \dot{\boldsymbol{\delta}}_s & \left(|k_s \boldsymbol{\delta}_s + \eta_s \dot{\boldsymbol{\delta}}_s| \le \mu |\boldsymbol{F}_{cn}|\right) \\ \mu |\boldsymbol{F}_{cn}| \dfrac{k_s \boldsymbol{\delta}_s + \eta_s \dot{\boldsymbol{\delta}}_s}{|k_s \boldsymbol{\delta}_s + \eta_s \dot{\boldsymbol{\delta}}_s|} & \left(|k_s \boldsymbol{\delta}_s + \eta_s \dot{\boldsymbol{\delta}}_s| > \mu |\boldsymbol{F}_{cn}|\right) \end{cases} \tag{14}$$

where k_n and k_s were the spring constants, η_n and η_s are the dashpot constants, $\boldsymbol{\delta}_n$ and $\boldsymbol{\delta}_s$ are the displacements, and $\dot{\boldsymbol{\delta}}_n$ and $\dot{\boldsymbol{\delta}}_s$ are the relative velocities in the normal and tangential directions, respectively, and μ is the friction coefficient. The k_n, k_s, η_n, η_s are set according to Hajivalie (2012). The $\boldsymbol{\delta}_s$ is calculated by integrating the relative velocity with respect to the point of contact as follows:

$$\boldsymbol{\delta}_s = \int_{t_c^0}^{t} \dot{\boldsymbol{\delta}}_s \, dt \tag{15}$$

where t_c^0 is the first contact time between solid particles i and j.

3.4.2 *Modeling of solid-fluid interaction*

E-MPS/DEM takes into account drag and lift forces as the $\boldsymbol{F}_f$ in Eq. (3). The drag force $\boldsymbol{F}_D$ is calculated as follows:

$$\boldsymbol{F}_D = \frac{1}{2}\rho_f A C_D |\boldsymbol{u}_f - \boldsymbol{u}_s|(\boldsymbol{u}_f - \boldsymbol{u}_s) \tag{16}$$

where ρ_f , A , C_D, $\boldsymbol{u}_f$, and $\boldsymbol{u}_s$ are the density of the fluid, projected area of the solid particles, drag coefficient, local average velocity vector of the fluid phase, and particle velocity vector, respectively. The C_D depends on the particle Reynolds number R_e and is calculated following Schiller and Naumann (1933) as follows:

$$C_D = \begin{cases} \frac{24}{Re}(1 + 0.15Re^{0.687}) & (Re \le 1000\ ) \\ 0.44 & (Re > 1000) \end{cases} \qquad Re = \frac{|\boldsymbol{u}_f - \boldsymbol{u}_s| d_s}{\nu} \tag{17}$$

where d_s is the sand-particle diameter. The lift force $\boldsymbol{F}_L$ is calculated as follows:

$$\boldsymbol{F}_L = \frac{1}{2}\rho_f A C_L |\boldsymbol{u}_f - \boldsymbol{u}_s|(\boldsymbol{u}_f - \boldsymbol{u}_s) \tag{18}$$

where C_L is the lift coefficient, which is 0.2. A local average velocity of the fluid phase for a solid particle is calculated as a weighted average as follows:

$$\boldsymbol{u}_{f\_i} = \frac{\sum_j^{fluid} \boldsymbol{u}_j\, w_s(|\boldsymbol{r}_j - \boldsymbol{r}_i|)}{\sum_j^{fluid} w_s(|\boldsymbol{r}_j - \boldsymbol{r}_i|)} \tag{19}$$

where $w_s(r)$ is the solid-fluid weight function. The weight function $w_s(r)$ in Eq. (19) can be written as follows:

$$w_s(r) = \begin{cases} 4\left(\frac{r}{r_e}\right)^5 - 5\left(\frac{r}{r_e}\right)^4 - 1 & (r < r_e) \\ 0 & (r < r_e) \end{cases} \tag{20}$$

With E-MSP/DEM, the solid particles composing the riverbed are treated as a wall, so that no fluid particles enter the riverbed. When $\boldsymbol{u}_f$ is calculated using Eq. (19) for a solid particle near the riverbed, it becomes an excessive quantity due to the average of only the fluid particles on the riverbed. Therefore, assuming that the fluid-phase flow velocity below the riverbed surface is 0, $\boldsymbol{u}_f$ in the horizontal direction to the riverbed surface is corrected as follows.

$$\boldsymbol{u}^h_{f\_i} = \frac{n_s}{n_{s0}}\boldsymbol{u}^h_{f\_i} \quad ; \quad \boldsymbol{u}^v_{f\_i} = \boldsymbol{u}^v_{f\_i} \tag{21}$$

where $\boldsymbol{u}^h_f$ and $\boldsymbol{u}^v_f$ are the horizontal and vertical direction components to the riverbed surface, respectively.

4. NUMERICAL EXAMPLE

4.1 Simulation setup

We conducted vertical two-dimensional numerical simulation for two cases in which the riverbed was located in the different area as shown Figures 4 (a) and (b). The scour downstream from the weir occurred with the lowering of the riverbed downstream. Therefore, in Case 1, the riverbed was set in the flat section with a 1-cm drop of the 1/12.5-slope section. In Case 2, the riverbed was set in the flat section and 1/12.5-slope section, as shown in Figure 4 (b). Table 1 lists the physical properties of the simulation. The q was 0.012 m^2/s, inflow

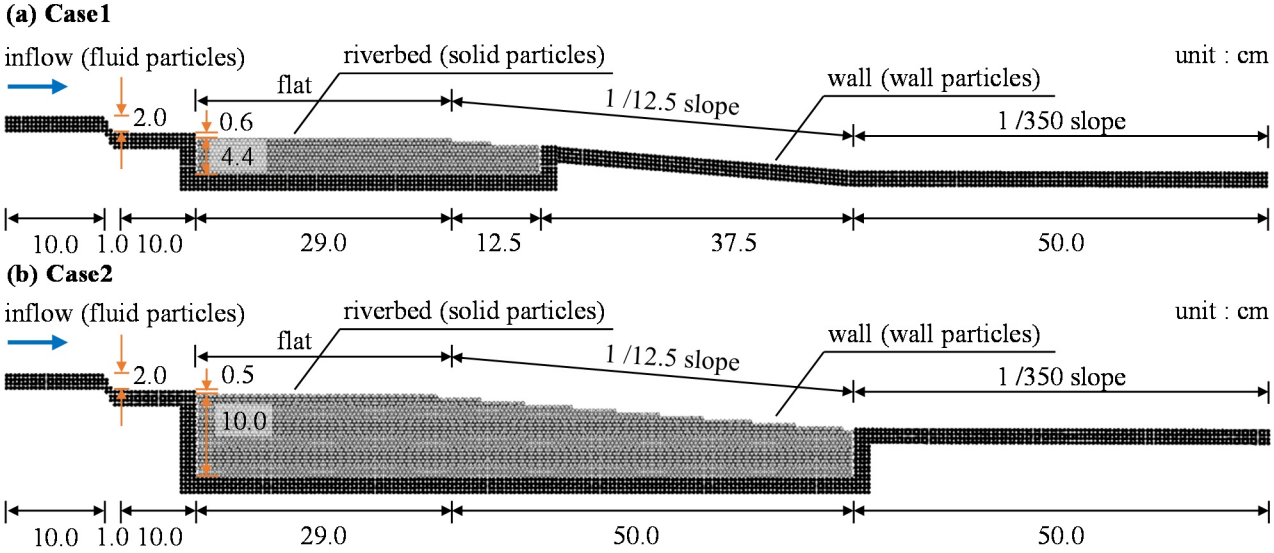

Figure 4. Computational domain

Table 1. Physical properties in the simulations

The E-MPS Fluid phase		The DEM solid phase	
d_f : Particle size (m)	5.0×10^{-3}	d_s : Particle diameter (m)	5.0×10^{-3}
r_e : Effective radius (m)	10.5×10^{-3}	R : Specific gravity in water of solid particles (-)	0.25
ρ_f : Fuluid density (kg/m^3)	1,000	k_n : Spring constant (normal) (N/m)	3.23×10^{2}
ν : Kinematic viscosity (m^2/s)	1.0×10^{-6}	k_s : Spring constant (tangential) (N/m)	1.24×10^{2}
c : Sound speed (m/s)	10.0	η_n : Dashpot constant (normal) (Ns/m)	1.45×10^{-1}
q : Unit width flow rate (m^2/s)	0.012	η_s : Dashpot constant (tangential) (Ns/m)	9.02×10^{-2}
		μ : Friction coefficient (-)	0.577

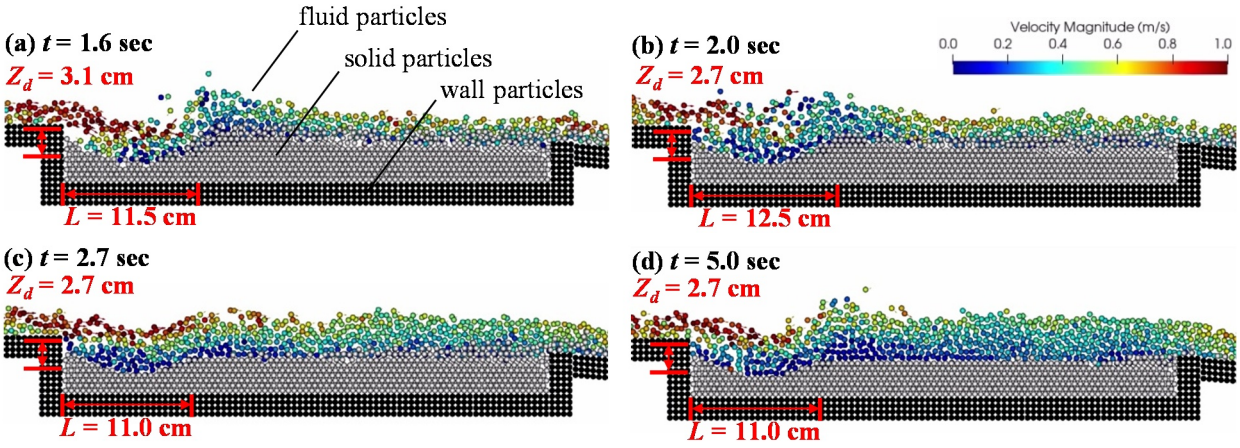

Figure 5. Numerical results for Case1

depth h_{in} was a critical depth of 2.5 cm, and inflow velocity v_{in} was given by q / h_{in}. The fluid particle size and solid particle diameter were set to 5 mm in relation to the calculation cost. The specific gravity in water of solid particles R was set to 0.25. The fluid force acting on a solid particle is proportional to the square of the particle diameter, as given by Eqs. (16) and (18). The acceleration of a solid particle is inversely proportional to the cube of the particle diameter, as given by Eq. (3). For the solid particles, the ratio of acting force and acceleration was made the same in the experiment and the simulation. The general R is 1.65. The R in the simulation was calculated by multiplying 1.65 by the sand particle diameter ratio of the experiment to the simulation. The calculation time interval Δt was set to 5.0×10^{-5} sec, and the simulation time was set to 20 sec in real time.

4.2 Results and discussion

4.2.1 Case1

Figures 5 (a)–(d) show the simulation results for Case 1. Figures 5 (a)–(d) show the flow conditions, riverbed conditions, z_d, and L, for 1.6, 2.0, 2.7, and 5.0 sec, respectively. The color of the fluid particles indicates the velocity magnitude of each particle. As in section 4.1, the riverbed changed faster during the simulation than during the experiment due to settings such as sand-particle diameter. The simulation results indicate that the jet flow changes to attached jet, wave jump, then attached jet, in a short time along with changes in the riverbed. This is a phenomenon that the scour progresses when the fluid and riverbed interact, which was confirmed from the experiment. On the other hand, the size of the scour during the simulation was approximately in a steady state at 2.7 sec, and the size was smaller than that in the experiment, as shown in Figures 5 (c)–(d). This is due to the fact that the simulation for Case1 is limited to the small riverbed; thus, the expansion of the scour was restricted.

4.2.2 Case2

Figure 6 shows the simulation results for Case 2 under flow conditions, riverbed conditions, z_d, and L for 20.0 sec. The color of the fluid particles indicates the velocity magnitude of each particle. The state of the riverbed at 20.0 sec during the simulation was in a steady state. Figure 7 shows the comparison of the riverbed surface between the 20.0-sec simulation and the 3 and 10 min of the experiment. The riverbed surface was measured from an image taken during the experiment. The scale of the scour during the simulation was about the same as that during the 3 min of the experiment, as shown in Figure 7. Although the scale of the scour during the simulation was smaller than that during the 10 min of the experiment, the simulation could capture the expansion phenomenon of the scour. Focusing on the riverbed surface downstream of the scour, the riverbed degradation during the simulation was larger than that during the experiment. E-MPS/DEM cannot take into ac count that once sand particles have left the riverbed, they are re-deposition and re-composition the riverbed. Excessive riverbed degradation downstream of the scour during the simulation may primarily be due to the

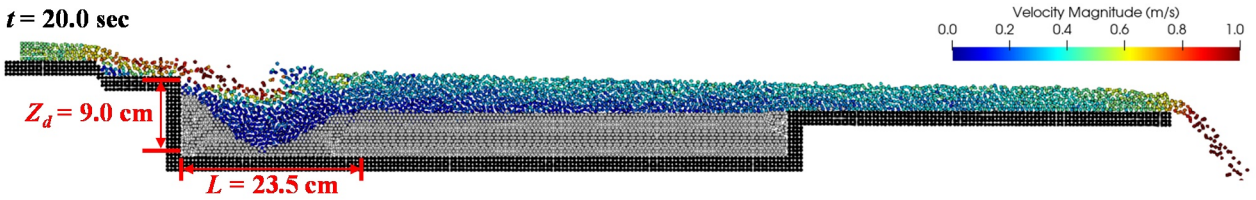

Figure 6. Numerical results for Case2

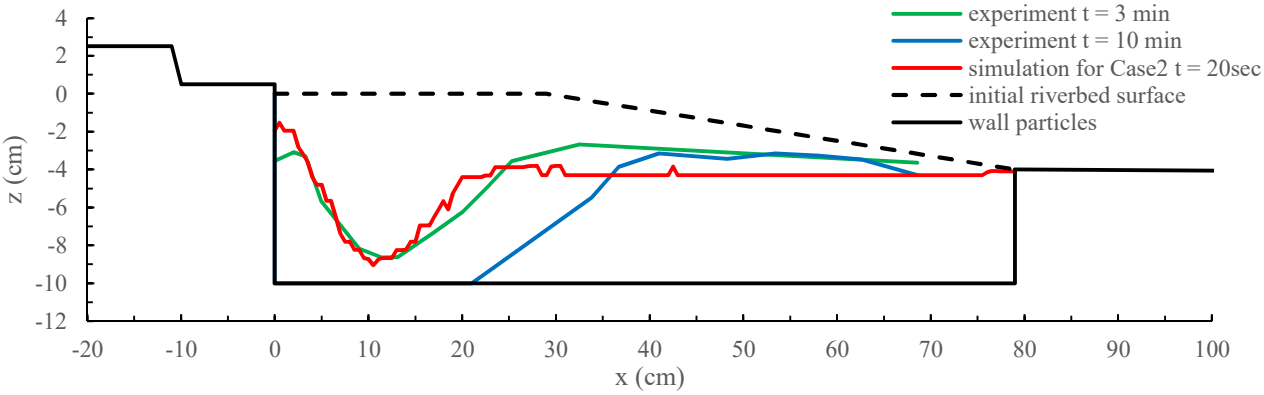

Figure 7. Comparison of sand bed surface between simulation and experiment for Case2

lack of expression of scoured sand particles re-deposition downstream. In the simulation, the water depth downstream of the scour increased, and the flow velocity downstream of the scour was evaluated to be small. Therefore, the scale of the scour during the simulation was considered smaller than that during the experiment.

5. CONCLUSIONS

The local scour phenomenon downstream of river crossing structures, such as weirs and groundsills, is a complex phenomenon that occurs when the fluid and riverbed interact. In this study, a coupling model of the E-MPS method and DEM (E-MPS/DEM) has been developed to overcome this difficult. In Case 1 of the simulation, E-MPS/DEM was able to reproduce the phenomenon of the jet flow changing due to changes in the riverbed in a short time, as in the experiment. E-MPS/DEM was shown to be reveal the scour phenomenon that occurs when fluid and riverbed interact. In Case 2, E-MPS/DEM was shown to reveal the expansion phenomenon of the scour, although there is room for improvement.

ACKNOWLEDGMENTS

This study was supported by the River Research and Development Institution under the Ministry of Land, Infrastructure, Transport and Tourism of Japan. The authors express their sincere appreciation.

REFERENCES

Cundall, P.A., and Strack, O.D.L. (1979). A discrete numerical model for granular assemblies. *Géotechnique*, 29 (1): 47–65.

Hajivalie, F., Yeganeh-Bakhtiary, A., Houshanghi, H., and Gotoh, H. (2012). Euler-Lagrange model for scour in front of vertical breakwater. *Applied Ocean Research*, 34: 96-106.

Harada, E., Gotoh, H., Ikari, H., and Khayyer, A. (2019). Numerical simulation for sediment transport using MPS-DEM coupling model. *Advances in Water Resources*, 129: 354-364.

Hoffmans, G.J.C.M. (1998). Jet scour in equilibrium phase. *Journal of Hydraulic Engineering*, 124(4): 430-437.

Koshizuka, S., and Oka, Y. (1996). Moving-particle semi-implicit method for fragmentation of incompressible fluid. *Nuclear Science and Engineering*, 123: 421–434.

Nakagawa, H., Tsujimoto, T., Shimizu, Y., and Murakami, S. (1987). Enlargement of the cavity due to sweeping of sands beneath bed protection as a cause of weir disaters. *Proceedings of the Japanese conference on hydraulics, JSCE*, 31: 359-364 (in Japanese).

Oochi, M., Koshizuka, S., and Sakai, M. (2010). Explicit MPS algorithm for free surface flow analysis. Transactions *JSCES 20100013* (in Japanese).

Oochi, M., Yamada, Y., Koshizuka, S., and Sakai, M. (2011). Validation of pressure calculation in Explicit MPS method. *Transactions JSCES*, 20110002 (in Japanese).

Schiller, V.L., and Naumann, A. (1933). Uber die grundlegenden berechnungen bei der scherkraftaufbereitung. *Z. verenines Deutscher Inge*, 77: 318-321.

Yamada, Y., and Sakai, M. (2013). Lagrangian-Lagrangian simulations of solid-liquid flows in a bead mill. *Powder Technology*, 239: 105-114.

Yamamoto, Y., Nakamura, R., and Suwa, Y. (2018). Research gaps suggested by hydraulic experiment of the deformation of block covered groundsill. *Advances in River Engineering, JSCE*, 23: 143-148 (in Japanese).